IEEE

SENSORS JOURNAL

JUNE 15, 2023 VOLUME 23 NUMBER 12 ISJEAZ (ISSN 1558-1748)

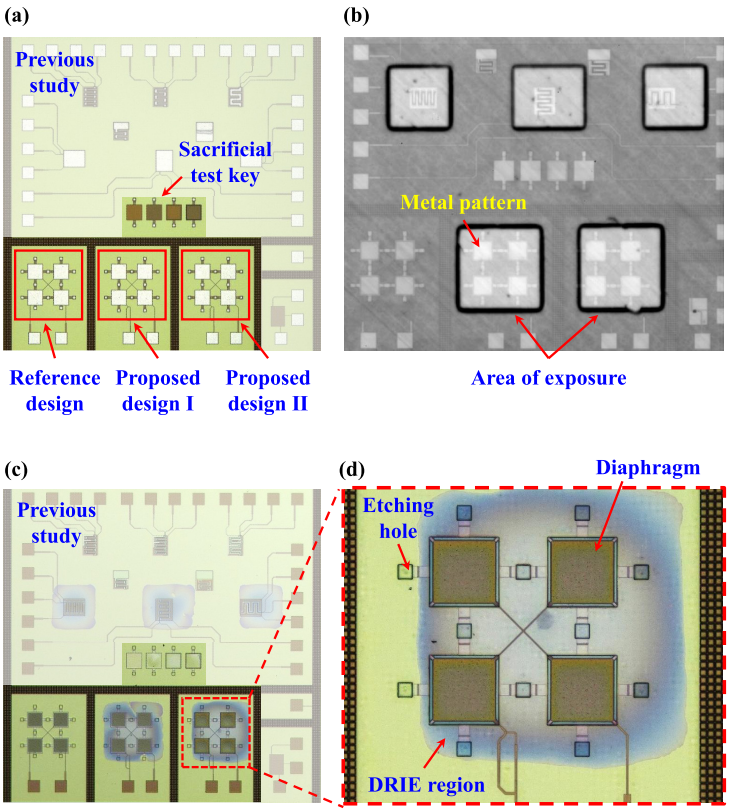

Optical micrographs to show (a) chip fabricated by the CMOS processes from the TSMC, (b) DRIE regions defined by the maskless photolithography (observed by the infrared optical microscope), (c) sensing chip after DRIE and metal wet-etching, and (d) zoomed-in view of the proposed pressure sensor array (vol. 22, no. 24, see page 23728).

IEEE Sensors Council

A PUBLICATION OF THE IEEE SENSORS COUNCIL
WWW.IEEE.ORG/SENSORS

IEEE

IEEE SENSORS JOURNAL

The IEEE SENSORS JOURNAL is published by the IEEE Sensors Council, which is sponsored by 26 IEEE societies (see the inside back cover). For membership and subscription information and pricing, please visit https://www.ieee.org/membership-catalog. *Member copies of Transactions/Journals are for personal use only.*

IEEE SENSORS JOURNAL (ISSN 1558-1748) is published semimonthly by The Institute of Electrical and Electronics Engineers, Inc. Responsibility for the contents rests upon the authors and not upon the IEEE, the Society/Council, or its members. **IEEE Corporate Office:** 3 Park Avenue, 17th Floor, New York, NY 10016. **IEEE Operations Center:** 445 Hoes Lane, Piscataway, NJ 08854. **NJ Telephone:** +1 732 981 0060. **Price/Publication Information:** Member and nonmember subscription prices available upon request.

Digital Object Identifier 10.1109/JSEN.2023.3281223

IEEE

SENSORS JOURNAL

JUNE 15, 2023 VOLUME 23 NUMBER 12 ISJEAZ (ISSN 1558-1748)

FEATURED ARTICLE

Magnetic Sensors

REVIEW ARTICLES

Mechanical Sensors

Sensor Applications

REULAR PAPERS

Chemical and Biological Sensors

(Contents Continued on Page 12428)

IEEE Sensors Council

A PUBLICATION OF THE IEEE SENSORS COUNCIL
WWW.IEEE.ORG/SENSORS

IEEE

(Contents Continued from Page 12427)

(Contents Continued on Page 12429)

(Contents Continued from Page 12428)

(Contents Continued on Page 12430)

(Contents Continued from Page 12429)

(Contents Continued on Page 12431)

(Contents Continued from Page 12430)

(Contents Continued on Page 12432)

(Contents Continued from Page 12431)

Integrated Microwave Sensor and Antenna Sensor Based on Dual T-Shaped Resonator Structures for Contact and Noncontact Characterization of Solid Material

Syah Alam, *Member, IEEE*, Zahriladha Zakaria, *Senior Member, IEEE*, Indra Surjati, *Member, IEEE*, Noor Azwan Shairi, *Member, IEEE*, Mudrik Alaydrus, *Senior Member, IEEE*, and Teguh Firmansyah, *Member, IEEE*

***Abstract*—This article proposes the integration of microwave sensors (MSs) and antenna sensors (ASs) for contact and noncontact characterization of solid materials. Integration between MS and AS was determined based on the reflection coefficient (S_{11}), where S_{11} of ≥ -10 dB was proposed as MS and S_{11} of ≤ -10 dB was proposed as AS. The proposed sensor consists of a dual T-shaped resonator with single port operating at a resonant frequency of $f_{r1} = 1.81$ GHz for MS and $f_{r2} = 2.34$ GHz for AS using FR-4 substrate with ε_r of 4.3, tanδ of 0.0265, and thickness of 1.6 mm. Furthermore, the two resonant frequencies had independent characteristics with different sensing hot spots. MS is proposed for permittivity detection of the material under test (MUT) for contact detection while non-contact detection is proposed by utilizing AS. The procedure for contact detection was carried out by placing the MUT on the surface of the sensor, while noncontact detection was carried out by placing the MUT with an air gap between the MUT (d) and the AS was 0.5–1.5 mm. The measurement results showed that the average accuracy was 99.30% and 99.31% for the MS and AS for the permittivity range of 1–6.15, while the normalized sensitivities (NSs) of the proposed sensors were 1.15% and 0.16%, respectively. The results of this research are novel and can be recommended for several purposes related to biomedical and pharmaceutical industries requiring contact and noncontact detection of material characterization.**

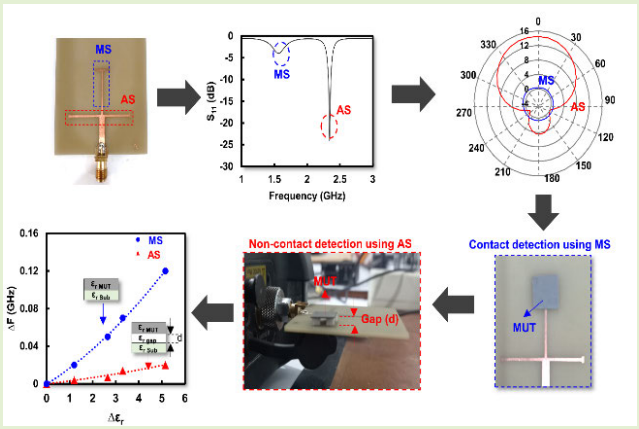

***Index Terms*— Antenna sensor (AS), contact detection, integrated, microwave sensor (MS), noncontact detection, solid material.**

I. Introduction

THE characterization of dielectric properties plays an important role in extracting the composition of materials for several applications, such as the biomedical industry [1], material science [2], and quality control [3]. Microwave sensor (MS) is recommended for material characterization because they have advantages, such as low cost, high accuracy, and applicable for noninvasive measurements [4]. Previous studies investigated the application of MS for the characterization of solid materials [5], [6], liquids [7], [8], and temperature [9], [10]. Generally, MS is used to detect permittivity [11], [12] by placing the material under test (MUT) on the surface of the sensing hot spot of the sensor. Several previous studies have proposed MS to characterize solid and liquid materials using complementary split ring resonator (CSRR) [13], [14], split ring resonator (SRR) [15], [16], planar inductor–capacitor (LC) resonators [17], interdigital capacitor (IDC) [18], [19], microstrip line ring resonator [20], and substrate integrated waveguide (SIW) [21], [22]. However, the structure of the previous sensors still uses a two-port configuration, so it has disadvantages such as being wasteful of resources and cannot be connected directly to wireless devices.

Manuscript received 26 March 2023; revised 2 May 2023; accepted 2 May 2023. Date of publication 10 May 2023; date of current version 14 June 2023. This work was supported in part by Universiti Teknikal Malaysia Melaka (UTeM) and Research Grants MTUNC/MC0011; and in part by Universitas Trisakti, Indonesia, through overseas research collaborations for fiscal years of 2022. The associate editor coordinating the review of this article and approving it for publication was Prof. Santosh Kumar. *(Corresponding authors: Syah Alam; Zahriladha Zakaria.)*

Please see the Acknowledgment section of this article for the author affiliations.

This article has supplementary downloadable material available at https://doi.org/10.1109/JSEN.2023.3273008, provided by the authors.

Digital Object Identifier 10.1109/JSEN.2023.3273008

Furthermore, a single port configuration MS has also been proposed to detect the permittivity of solid materials using a U-shaped resonator [23], slot-loaded microstrip [24], and aperture coupling [25]. The advantages of MS with a single port are having independent characteristics, a simpler structure, more economical resources, and having a hybrid function as an antenna, so that it can be used to transmit data using a wireless network. Generally, material characterization using MS is carried out by placing the MUT in direct contact, so that it can reduce the performance of the sensor. This caused the surface of the sensor to potentially be damaged due to oxidation and corrosion. To overcome this limitation, noncontact detection is proposed as a solution to make the sensor more durable, accurate, and sterile.

Noncontact detection using MS by utilizing the electric (**E**-) and magnetic (**H**)-fields from the resonator has been proposed to characterize several materials [26], [27], [28]. Previous research conducted by Yang et al. [29] proposed noncontact detection for complex permittivity and thickness of solid materials using a single-compounded triple complementary resonator SRR with a maximum gap of 0.2 mm. Furthermore, the research proposed by Ali et al. [30] described noncontact detection for permittivity and thickness detection of MUT for solid materials using an IDC resonator with a gap of 0.3 mm. However, the gap between the MUT and the sensor was still limited and reduced the performance and sensitivity of the sensor. Another study by Wu and Wang [31] proposed noncontact detection with an antenna based on an artificial magnetic conductor (AMC) array for permittivity detection of water and ethanol in oil. Furthermore, the research presented by [33] proposed a microwave active antenna sensor (AS) for sensing liquid properties. However, the measurement process required the antenna interrogator to detect the permittivity of the MUT.

Based on the previous research i [23], [24], [25], it can be concluded that contact detection has several advantages, such as high accuracy and high sensitivity, but the limitation is that the surface of the sensor has the potential to be damaged due to oxidation and corrosion. On the other hand, noncontact detection based on [29], [30], [31], and [32] had the advantage that the sensor is more durable, and the surface of the sensor is more sterile. However, the limitations of noncontact detection are that the performance and sensitivity are greatly affected by the distance between the sensor and the material. Therefore, the combination of the MS and AS is an excellent solution for material characterization both in contact and noncontact detection to maintain the performance of the sensor.

This article has the advantage of integrating contact and noncontact detection for the characterization of solid materials based on MS and AS. The sensors are proposed using dual T-shaped resonators with a single port that operate at two different resonant frequencies at $f_{r1} = 1.81$ GHz and $f_{r2} = 2.35$ GHz for MS and AS, respectively. Furthermore, the proposed sensor has independent characteristics and different sensing hot spot locations for contact and noncontact detection, so that the characterization of the MUT can be carried out separately, where the low frequency (f_{r1}) is used as MS for noncontact detection, while high frequency (f_{r2}) is used as AS. The proposed sensor has been successfully simulated, modeled using electromagnetic simulation, and validated by the measurement process. The range of permittivity detected is 1–6.15 for MS and AS, respectively. Furthermore, the sensitivity of the AS with noncontact detection can be evaluated based on the air gap (d) of 0.5–1.5 mm.

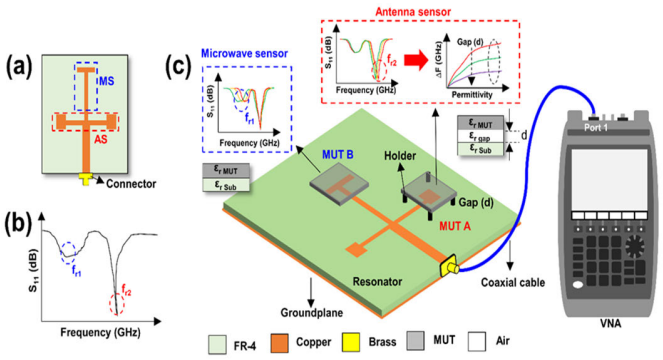

Fig. 1. (a) Structure of the proposed resonator. (b) Resonant frequency of the proposed resonator. (c) Scenario of contact and noncontact detection using MS and AS.

II. Working Principle of the Proposed Sensors

A. Scenario of Contact and Noncontact Detection Using MS and AS

The proposed sensor consists of dual T-shaped resonators with a single port operating at two resonance frequencies, the first resonator is $f_{r1} = 1.81$ GHz and the second resonator is $f_{r2} = 2.35$ GHz, as shown in Fig. 1(a). The low frequency is proposed as MS, while the high frequency is proposed as AS, as shown in Fig. 1(b). The proposed resonator has independent characteristics with different sensing hot spots, so that contact and noncontact detection can be carried out separately. Furthermore, the measurement process was carried out using a vector network analyzer (VNA), where the proposed sensor was connected using a coaxial cable with an impedance of 50 Ω.

MS and AS were determined based on the frequency shift on the reflection coefficient (S_{11}), where S_{11} of ≥ -10 dB was proposed as MS and S_{11} of ≤ -10 dB was proposed as AS. The sensing hot spot was determined based on the concentration of the **E**- and **H**-fields of each resonator. Furthermore, the surface of the resonator which had a high concentration of **E**-field and a low concentration of **H**-field was used as an MS for contact detection. On the other hand, noncontact detection utilized the surface of the resonator, which has the same location as **E**- and **H**-fields. Generally, resonators that function as antennas transmit electromagnetic waves, where the **E**- and **H**-fields were in the same location; therefore, it can be utilized for AS. The permittivity of the MUT was observed based on the shift in the resonant frequency of the resonator when the MUT was placed at each sensing hot spot. Fig. 1(c) shows a scenario of a contact and noncontact detection using MS and AS, where the permittivity of the MUT was ε_r MUT, the air gap was ε_r gap (vacuum = 1), and the substrate of the resonator was ε_r sub.

Furthermore, for contact detection, the MUT was positioned directly without an air gap on the top surface of the first

TABLE I
DIMENSIONS OF DUAL T-SHAPED RESONATOR

Parameter	Value	Parameter	Value
W_z	3 mm	W_d	2 mm
L_z	15 mm	W_t	1 mm
L_a	16 mm	L_t	18 mm
L_b	3 mm	W_s	1 mm
L_c	15 mm	L_s	8 mm
L_d	16 mm	W_g	50 mm
W_c	13 mm	L_g	50 mm

resonator as MS. Moreover, noncontact detection was proposed by separating the MUT from the top surface of the resonator using an air gap with a range of 0.5–1.5 mm using AS. It should be noted that the distance between the air gap and the sensor greatly affected the frequency shift (ΔF), sensitivity, and performance of the AS.

B. Design of Dual T-Shaped Resonator

The proposed sensor was designed using an FR-4 substrate with a permittivity of 4.3, a loss tan of 0.0265, and a thickness (h) of 1.6 mm. The structure and dimensions of the proposed sensor are shown in Fig. 2(a) and (b) using a dual T-shaped resonator connected directly to the sub miniature version A (SMA) connector via a microstrip line with an impedance of 50 Ω.

Furthermore, the equivalent circuit (EQC) model using R as resistors, L as inductors, and C as capacitors of the proposed resonator is shown in Fig. 2(c), where the first resonator is represented by $R_2 = 0.379$ kΩ, $L_2 = 5.530$ nH, and $C_2 = 1.530$ pF, while the second resonator is represented by $R_1 = 1.341$ kΩ, $L_1 = 3.010$ nH, and $C_1 = 1.160$ pF. To control the impedance of the resonator, the transmission line was modeled and represented by $Z_1 = 50$ Ω with $\theta = 55.40$, which was connected to port 1 with an impedance of 50 Ω. Furthermore, $C_{g1} = 0.299$ pF and $C_{g2} = 0.378$ pF were proposed to prevent a short circuit between the resonator and the connector. The overall dimensions of the proposed sensor are shown in Table I.

In this article, the modeling of EQCs is simulated using AWR Office 2009, while finite element modeling (FEM) used high frequency structure simulator (HFSS) 15.0. A comparison of the simulation results between the FEM and EQC models of the proposed resonator obtained consistent results, where the resonator operated at two resonant frequencies $f_{r1} = 1.57$ GHz and $f_{r2} = 2.35$ GHz, as shown in Fig. 2(d). Based on the theory, the resonant frequency of the resonator can be determined using the following [36]:

$$f_o = \frac{1}{2\pi\sqrt{L_n C_n}} \tag{1}$$

where the capacitors (C_n) and inductors (L_n) are used to control the resonant frequency (f_o), while resistors (R_n) are used to control S_{11} of the resonator.

C. Working Principle of Contact and Noncontact Detection

Contact and noncontact detection using MS and AS can be modeled using EQCs using a resistor (R), capacitor (C), and inductor (L). Each component describes the physical mechanisms that arise in E- and H-fields, and the quantitative value of each component is simulated and extracted using AWR MWO 2009. Furthermore, for contact detection, the permittivity of MUT was assumed to be a capacitive load connected in parallel with the capacitors of the resonator, where C_{sub} and C_{MUT} represent the capacitance of the resonator and MUT [33]. On the other hand, for noncontact detection, C_{MUT} was connected in series with C_{gap}. The EQC models of contact and noncontact detection using MS and AS are shown in Fig. 3(a) and (b).

Furthermore, the structure of the contact detection using MS consists of two layers: ε_{r1} and ε_{r3}, which represent the permittivity of the resonator and MUT, as shown in Fig. 3(a), respectively. The structure of the noncontact detection using AS consisted of three layers: ε_r sub, ε_r gap, and ε_r MUT, as shown in Fig. 3(b), representing the permittivity of the resonator, gap, and MUT, respectively. In this article, an air gap was proposed to separate the sensor and MUT with a permittivity of ε_r gap $= 1$. The total capacitance of contact and noncontact detection is represented by $C_{T\,\text{co}}$ and $C_{T\,\text{nco}}$,

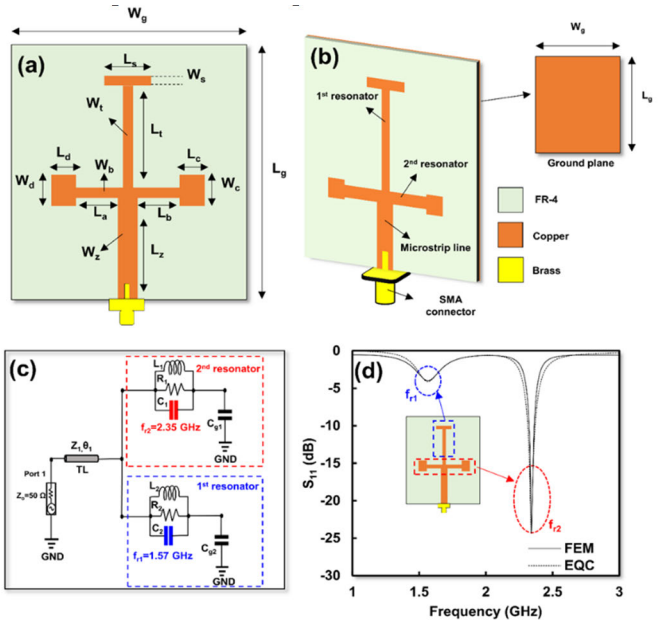

Fig. 2. (a) Design of dual T-shaped resonator and (b) perspective view. (c) EQC model of the proposed resonator. (d) Simulation of the proposed resonator based on FEM and EQC.

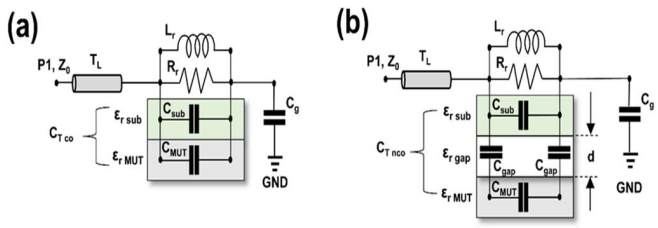

Fig. 3. EQC model of (a) contact detection using MS and (b) noncontact detection using AS with an air gap.

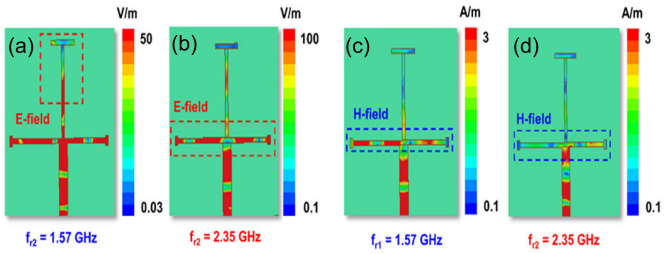

Fig. 4. Simulation result of **E**- and **H**-field concentration. **E**-field at (a) $f_{r1} = 1.57$ GHz and (b) $f_{r2} = 2.35$ GHz. **H**-field at (c) $f_{r1} = 1.57$ GHz and (d) $f_{r2} = 2.35$ GHz.

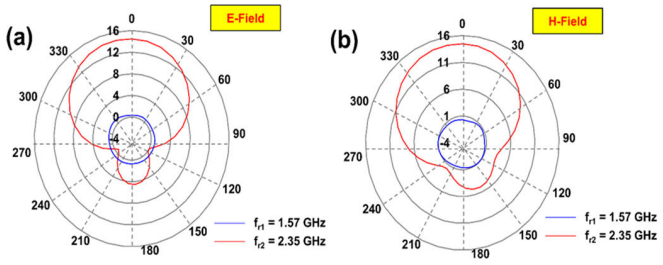

Fig. 5. Radiation pattern of the proposed resonator. (a) **E**-plane at $f_{r1} = 1.57$ GHz and $f_{r2} = 2.35$ GHz. (b) **H**-plane at $f_{r1} = 1.57$ GHz and $f_{r2} = 2.35$ GHz.

which can be determined by the following equation:

$$C_{T\,\mathrm{co}} = C_{\mathrm{Sub}} + C_{\mathrm{MUT}} \tag{2}$$

$$C_{T\,\mathrm{nco}} = C_{\mathrm{Sub}} + \frac{C_{\mathrm{gap}}.C_{\mathrm{MUT}}}{C_{\mathrm{gap}} + C_{\mathrm{MUT}}}. \tag{3}$$

Equations (2) and (3) show that the value of $C_{T\,\mathrm{co}}$ is higher than $C_{T\,\mathrm{nco}}$, and this causes a shift in the frequency for contact detection to be higher than noncontact detection. It should be noted that C_{gap} can be assumed as the distance between the MUT and the sensor (d), where the value of C_{gap} will increase for a small air gap and vice versa. Moreover, by placing the MUT both in contact and noncontact with the air gap, the resonant frequency of the resonator changes. The permittivity of the MUT can be determined from the frequency shift of the resonator. Furthermore, the resonant frequency of MS (f_{ms}) and AS (f_{as}) for contact and noncontact detection can be determined as follows:

$$f_{\mathrm{ms}} = \frac{1}{2\pi\sqrt{L_r(C_{\mathrm{sub}} + C_{T\,\mathrm{co}})}} \tag{4}$$

$$f_{\mathrm{as}} = \frac{1}{2\pi\sqrt{L_r(C_{\mathrm{sub}} + C_{T\,\mathrm{nco}})}}. \tag{5}$$

It should be noted that the frequency shift of AS was greatly influenced by the distance between the sensor and the MUT, which is represented as d. Therefore, the gap between the resonator and the MUT needs to be evaluated to obtain the best sensitivity and performance of sensor.

D. Sensing Hot Spot Location of MS and AS

The sensing hot spot was determined based on the concentration of the **E**- and **H**-fields at each resonator. Both resonators had different **E**- and **H**-fields concentrations based on their respective resonant frequencies. The permittivity of the MUT was detected by placing the material at the sensing hot spot location. The simulation results of the **E**- and **H**-field concentrations are shown in Fig. 4(a)–(d).

Based on the simulation results using HFSS 15.0, the concentration of the **E**-field of the first resonator with $f_{r1} = 1.57$ GHz is in the open-ended stub, while the **H**-field is in the middle arm of the second resonator, as shown in Fig. 4(a) and (c). These results show that the first resonator can function as MS with the sensing hot spot located on the open-ended stub. On the other hand, the **E**-field and **H**-field concentrations of the second resonator with $f_{r2} = 2.35$ GHz were in the same location on the middle arm of the proposed sensor, as shown in Fig. 4(b) and (d). These results indicate that the second resonator can function as AS with a sensing hot spot location on the middle arm of the proposed device, where the maximum concentration of **E**- and **H**-fields was obtained. To validate the function of both resonators, a simulation of the radiation pattern was proposed to observe the performance of each, as shown in Fig. 5(a) and (b).

The simulation of the radiation pattern of the **E**- and **H**-fields of both resonators showed that the second resonator had maximum radiation compared to the first resonator. These results confirmed that the second resonator can be proposed as AS, while the second resonator can be proposed as MS.

III. Simulation of the Proposed Sensor

The simulation process was carried out using HFSS 15.0, where two scenarios were proposed to detect the permittivity of MUTs both in contact and noncontact.

1) MUT was placed on the sensing hot spot of the first resonator directly without an air gap as MS for contact detection, while the second resonator is in a vacuum.
2) MUT is placed on the sensing hot spot of the second resonator with an air gap as AS for noncontact detection, while the first resonator is in a vacuum.

The simulation results of MS and AS with a permittivity range of 1–10 are shown in Fig. 6(a) and (b), respectively. The resonant frequency of MS (f_{r1}) moves to the lower frequency from 1.770 to 1.570 GHz, while f_{r2} does not shift significantly while scenario 1) is applied, as shown in Fig. 6(c). Furthermore, the same characteristics were also obtained for the AS, where f_{r2} moved to the lower frequency from 2.355 to 2.322 GHz when the MUT was placed in noncontact with an air gap (d) of 0.5 mm, as shown in Fig. 6(d), while f_{r1} does not shift significantly while scenario 2) is applied. This indicated that the two resonators had independent characteristics both in contact and noncontact detection.

The ratio between the frequency shift and the change in the permittivity of the MUT was expressed as sensitivity. The sensitivity of the sensor was calculated using the following equation [30]:

$$S = \frac{\Delta f}{\Delta \varepsilon_r} = \frac{(f_{\mathrm{unloaded}} - f_{\mathrm{loaded}})}{\varepsilon_{r(\mathrm{MUT})} - \varepsilon_{r(\mathrm{Reference})}} \tag{6}$$

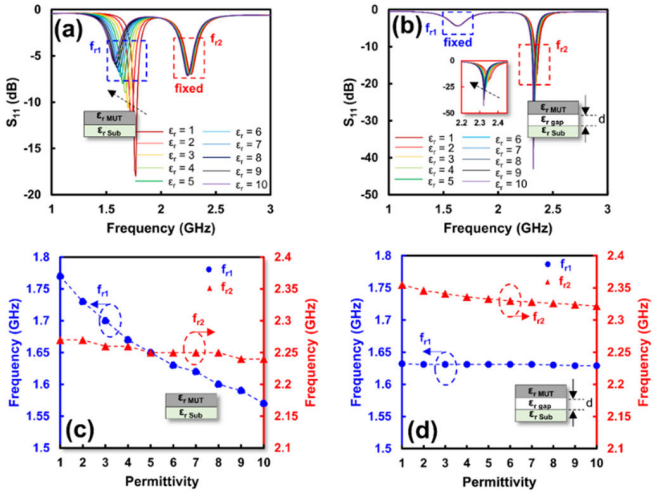

Fig. 6. Simulation results of the proposed resonator at (a) f_{r1} = 1.57 GHz as MS for contact detection and (b) f_{r2} = 2.35 GHz as AS for noncontact detection with an air gap of 0.5 mm. Correlation between f_{r1} and f_{r2} for (c) MS and (d) AS.

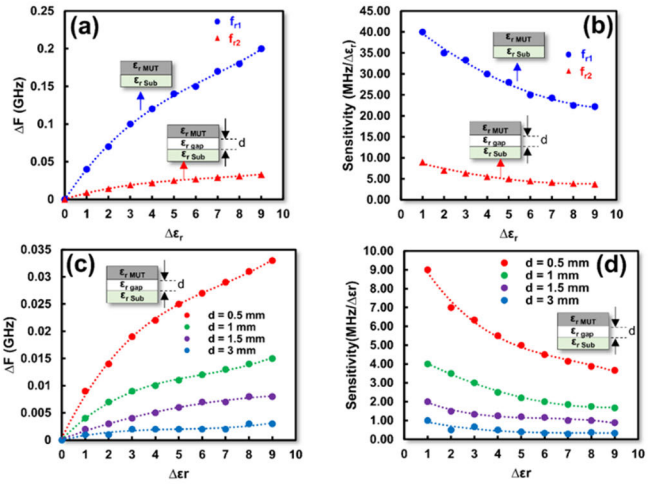

Fig. 7. (a) ΔF of MS and AS for contact and noncontact detection. (b) Sensitivity of MS and AS. Effect air gap of AS with (c) ΔF and (d) sensitivity.

where S is the sensitivity of the sensor, and ΔF is the difference between the loaded and unloaded resonant frequency. The sensitivity of MS and AS is shown in Fig. 7(a) and (b), where the MS has a maximum sensitivity of 40 MHz/$\Delta\varepsilon_r$ and ΔF of 0.2 GHz/$\Delta\varepsilon_r$, while AS is 9 MHz/$\Delta\varepsilon_r$ and ΔF of 0.033 GHz/$\Delta\varepsilon_r$. These results indicate that MS was more sensitive than AS.

Furthermore, other findings showed that ΔF and the sensitivity of AS for noncontact detection were greatly affected by the distance from the air gap (d), as shown in Fig. 7(c) and (d). From the simulation results with an air gap of 0.5–3 mm, the sensitivity range was 3.67–9 MHz/$\Delta\varepsilon_r$, while for ΔF was 0–0.033 GHz/$\Delta\varepsilon_r$. In other words, AS was more sensitive for noncontact detection with small air gaps. The effect of changes in tanδ on both resonators was simulated and observed in this article. Fig. 8(a) and (b) shows that

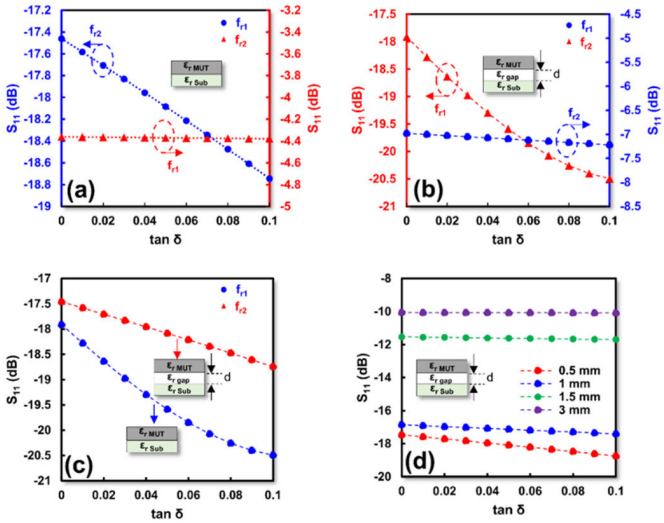

Fig. 8. Effect of tanδ for (a) MS and (b) AS with an air gap of 0.5 mm. (c) Comparison result effect of tanδ from MS and AS with an air gap of 0.5 mm. (d) Effect an air gap of AS with tanδ.

changes in tanδ with a range of 0–0.1 greatly affected the S_{11} of the resonator.

Based on the simulation, MS had a better sensitivity for detecting changes in tanδ compared to AS, as shown in Fig. 8(c), with a shift in S_{11} from −17.91 to −20.49 dB for contact detection, while non-contact detection is from −17.46 to −18.74 dB. In addition, the two sensors had independent characteristics both with MS and AS. Another finding is that the gap between the sensor and the MUT of AS greatly affected the value of S_{11}, as shown in Fig. 8(d), where S_{11} increased for small gap distances. Furthermore, S_{11} of AS shifted from −17.46 to −10.06 dB in line with changes in the air-gap distance between the sensor and the MUT in the range of 0.5–3 mm. The best performance of AS was obtained with an air gap of 0.5 mm.

IV. Measurement and Verification

A. Fabrication and Measurement Scenario for MS and AS

The fabrication of the proposed device and MUT is shown in Fig. 9(a), where the MUTs used were RO5880 (ε_r = 2.2 and tanδ = 0.009), RO4003C (ε_r = 3.65 and tanδ = 0.0027), FR-4 (ε_r = 4.3 and tanδ = 0.0265), and RO3006 (ε_r = 6.15 and tanδ = 0.0025) with dimensions of 10 × 10 × 1.6 mm. The measurement process was carried out using VNA, which was connected directly to the proposed sensor using an SMA connector via port 1 with an impedance of 50 Ω, as shown in Fig. 10(a). The frequency range used was 1.00–3.00 GHz with a sweep frequency of 0.001 GHz and an ambient temperature of 25 °C. The measurement data were stored using a universal serial bus (USB) device connected to a VNA and were processed using a personal computer (PC).

A comparison of the simulation and measurement of the proposed resonator is shown in Fig. 9(b), where the two resonators had identical characteristics as dual-band resonators. However, there were still errors and frequency shifts, where

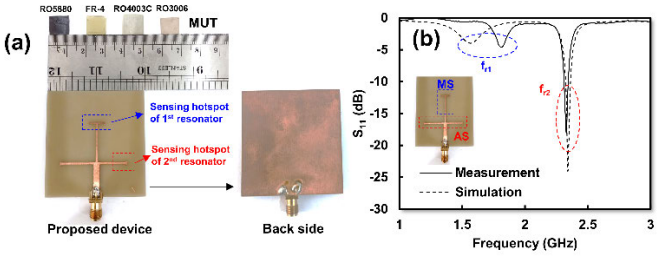

Fig. 9. (a) Fabricated of the proposed resonator. (b) Simulation versus measurement of the proposed resonator.

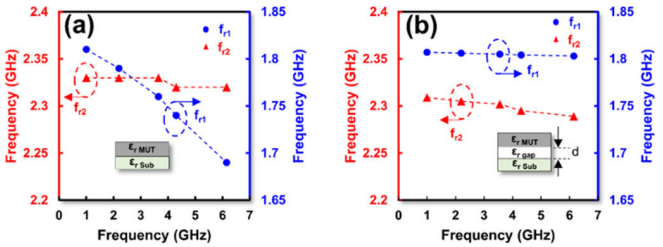

Fig. 11. Independent performance of (a) MS for contact detection and (b) AS for noncontact detection with an air gap of 0.5 mm.

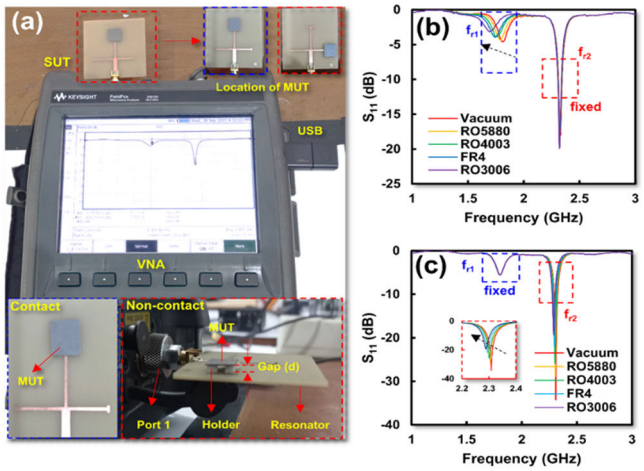

Fig. 10. (a) Placement scenario of MUT. Measurement result of (b) contact detection using MS and (c) noncontact detection using AS with an air gap of 0.5 mm.

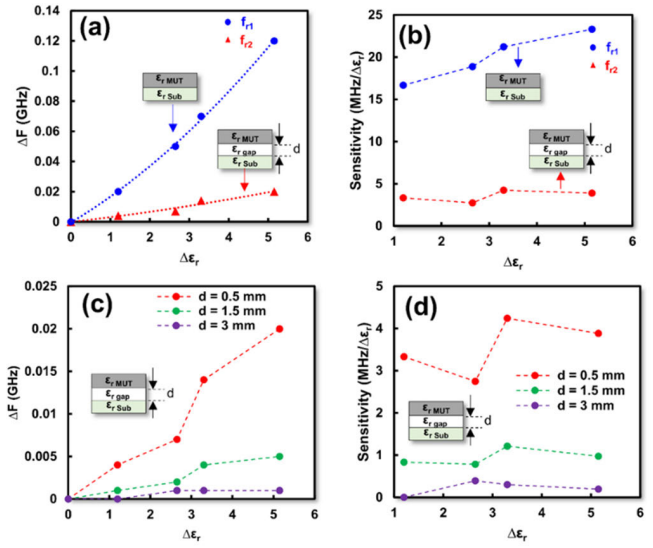

Fig. 12. (a) Comparison of sensitivity for MS and AS. (b) Correlation between air gap and sensitivity for AS. (c) Comparison of ΔF for MS and AS. (d) Correlation between air gap and ΔF for AS.

f_{r1} shifts from 2.35 to 2.34 GHz, while f_{r2} shifts from 1.57 to 1.81 GHz. This was due to the variation of permittivity in the substrate, namely, the range of ε_r of 4.25–4.35, and the error during the fabrication process.

To validate and measure the performance of MS and AS for contact and noncontact detection, two scenarios, as shown in Fig. 10(a), were proposed.

1) MUT was placed on the sensing hot spot of the first resonator without an air gap as MS for contact detection, while the second resonator was in a vacuum.
2) MUT was placed on the sensing hot spot of the second resonator with an air gap as AS for noncontact detection, while the first resonator was in a vacuum.

Based on the measurements, for scenario 1), f_{r2} shifted to the lower frequency when the permittivity of the MUT increased, while f_{r1} was fixed. The same characteristics were obtained for scenario 2), where f_{r1} shifted to the lower frequency, while f_{r2} was fixed for the permittivity range 1–6.15, as shown in Fig. 10(b) and (c). The independent performance of the resonators is shown in Fig. 11(a) and (b), where the respective resonant frequencies of the two resonators did not experience a significant shift when they were used as MS and AS for contact and noncontact detection with the permittivity range of 1–6.15.

For contact detection using MS, f_{r1} shifted from 1.810 to 1.690 GHz, while f_{r2} shifted slightly from 2.340 to 2.320 GHz. Furthermore, for AS, f_{r1} shifted from 2.309 to 2.289 GHz, while f_{r1} shifted slightly from 1.807 to 1.804 GHz. These results also proved that MS is more sensitive than AS. Another interesting finding, the two resonators had independent characteristics and these results are in line with the simulation process.

TABLE II
PERFORMANCE OF THE PROPOSED MS AND AS WITH AN AIR GAP OF 0.5 MM

MUT	MS			AS		
	ΔF (GHz/Δε$_r$)	S (MHz/Δε$_r$)	Acc. (%)	ΔF (GHz/Δε$_r$)	S (MHz/Δε$_r$)	Acc. (%)
Vacuum	-	-	98.001	-	-	99.641
RO5880	0.020	16.161	99.091	0.004	3.330	99.842
RO4003C	0.050	18.862	99.732	0.007	2.741	97.170
FR-4	0.070	21.213	99.772	0.014	4.240	99.932
RO-3006	0.120	23.301	99.843	0.020	3.882	99.953

B. Sensitivity and Accuracy of MS and AS for Contact and Noncontact Detection

The effect of the air gap with ΔF and the sensitivity is also discussed in this article. The maximum sensitivity of

TABLE III
COMPARISON OF THE PROPOSED SENSOR BASED ON PREVIOUS LITERATURE

Ref	Model	Range of permitivitty (ε_r)	Material Under Test (MUT)	Resonance frequency (GHz)			Independent perfomance	Num. of port	Range of gap (mm)	Contact	Non-contact	Integrated Function MS & AS	Design complexity
				f_{r1}	f_{r2}	f_{r3}							
[34]	Couple line section	1 – 10.2	Solid	1.50	-	-	No	2	-	Yes	No	No	High
[35]	SRR	1 – 3	Solid	2.65	-	-	No	2	-	Yes	No	No	Moderate
[17]	LC resonators	1 – 10.2	Solid	2.00	-	-	No	2	-	Yes	No	No	High
[20]	Microstrip line ring resonator	1 – 3.48	Solid	4.89	9.81	-	No	2	-	Yes	No	No	High
[23]	Dual U-Shaped resonator	1 – 4.3	Solid	1.21	2.10	-	Yes	1	-	Yes	No	No	Moderate
[25]	Aperture Coupling	1 – 12.85	Solid	9.50	12.30	-	No	1	-	Yes	No	No	High
[36]	CSRR resonator	1 – 11.90	Solid	5.35	7.99	-	No	2	-	Yes	No	No	Moderate
[24]	Slot loaded	1 – 10.2	Solid	2.50	-	-	No	1	-	Yes	No	No	Moderate
[29]	SC-TCSRR	1 – 4.4	Solid	1.42	2.65	4.40	No	2	0.10 – 0.50	No	Yes	No	Moderate
[30]	IDC	3 – 6	Solid	1.38	-	-	No	2	0.02 – 0.30	No	Yes	No	High
This work	Dual T-Shaped	1 – 6.15	Solid	1.52	2.35	-	Yes	1	0.50 – 1.50	Yes	Yes	Yes	Low

MS was 23.30 MHz/$\Delta\varepsilon_r$ with ΔF of 0.12 GHz/$\Delta\varepsilon_r$ while that of AS was 4.24 MHz/$\Delta\varepsilon_r$ and 0.02 GHz/$\Delta\varepsilon_r$ with an air gap of 0.5 mm, as shown in Fig. 12(a) and (b). The air-gap distance (d) greatly affected the sensitivity and ΔF of the AS, as shown in Fig. 12(c) and (d). The maximum sensitivity and ΔF of the AS with a gap of 0.5–1.5 mm were in the range of 0.001 GHz GHz/$\Delta\varepsilon_r$–0.02 GHz GHz/$\Delta\varepsilon_r$ and 0.39 MHz/$\Delta\varepsilon_r$–4.24 MHz/$\Delta\varepsilon_r$, respectively. This finding is in line with the simulation results, where the AS is more sensitive with smaller air gaps.

Furthermore, the difference between the permittivity of the MUT and the reference is expressed as $\Delta\varepsilon_r$. Generally, the reference permittivity used is a vacuum with $\varepsilon_r = 1$. The normalized sensitivity (NS) was calculated by the following equation [26]:

$$\mathrm{NS} = \frac{1}{\Delta\varepsilon_r}\left(\frac{f_{\mathrm{unloaded}} - f_{\mathrm{loaded}}}{f_{\mathrm{unloaded}}}\right)\%. \tag{7}$$

Based on (7), the NS of the proposed MS and AS sensor was 1.15% and 0.16% with a permittivity range of 1–6.15. Furthermore, the accuracy of MS and AS for contact and noncontact detection was obtained by using the polynomial equations. The permittivity from the datasheet was used as a reference and was compared to the permittivity calculated based on the polynomial equation. The comparison of the permittivity values from the datasheet and the calculation from MS and AS are shown in Fig. 13(a) and (b).

Based on measurements and calculations, the permittivity of the MUT was determined for MS (ε_{r1}) and AS (ε_{r2}) with the following equation:

$$\varepsilon_{r1} = a_1 {f_{\mathrm{ms}}}^4 - a_2 {f_{\mathrm{ms}}}^3 + a_3 {f_{\mathrm{ms}}}^2 - a_4 f_{\mathrm{ms}} + a_5 \tag{8}$$

$$\varepsilon_{r2} = b_1 {f_{\mathrm{as}}}^4 - b_2 {f_{\mathrm{as}}}^3 + b_3 {f_{\mathrm{as}}}^2 - b_4 f_{\mathrm{as}} + b_5 \tag{9}$$

where f_{ms} is the resonant frequency of MS with $a_1 = 41\,667$, $a_2 = 294\,643$, $a_3 = 780\,982$, $a_4 = 919\,666$, and $a_5 = 405\,977$, as shown in (8). On the other hand, f_{as} represented the resonant frequency of AS with $b_1 = 4 \times 10^8$, $b_2 = 3 \times 10^9$, $b_3 = 1 \times 10^{10}$, $b_4 = 2 \times 10^{10}$, and $b_5 = 1 \times 10^{10}$, as shown in (9). Table II shows the accuracy of permittivity detection for MS and AS for permittivity from 1 to 6.15. From the measurement results, the average accuracy of the MS and AS with an air gap of 0.5 mm is 99.30% and 99.31%, respectively. These results indicate that both sensors had high accuracy in detecting the permittivity of the MUT. The overall performance of MS and AS including sensitivity and ΔF and accuracy is shown in Table II.

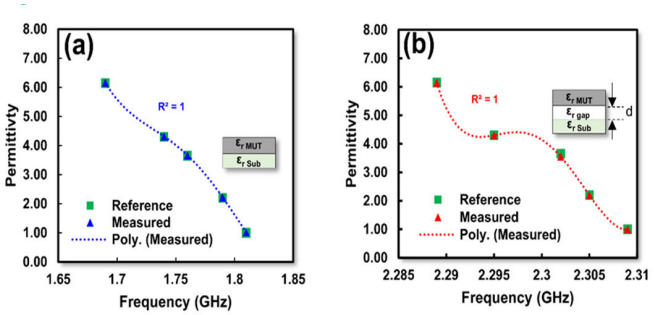

Fig. 13. Accuracy of (a) MS compared with reference permittivity and (b) AS compared with reference permittivity.

Table III shows that the performance of MS was more sensitive than AS with an air gap of 0.5 mm. Furthermore, both sensors had high accuracy and independent characteristics for both MS and AS for contact and noncontact detection.

V. EXPERIMENTAL VALIDATION WITH THE EXISTING SENSORS

In this article, integrated MS and AS based on dual T-shaped resonators are presented. MS and AS were proposed for permittivity detection of MUT for contact and noncontact detection, respectively. In addition, this article introduces a dual T-shaped resonator structure that has independent

characteristics using a single port. The proposed sensor also has two different sensing hot spots, so that it can be proposed for contact and noncontact measurements independently. Table III shows a comparison between the proposed work and the existing sensors.

Table III presents that the proposed device has novelty by proposing integration of MS and AS. Another novelty, the dual T-shaped resonator has independent characteristics, so that it can be used for contact and noncontact detection independently. Moreover, this study also presents the correlation between the distance from the air gap to the accuracy and sensitivity of AS for noncontact detection. Based on the measurements, an air gap (d) of 0.5–1.5 mm is proposed to separate the sensor and MUT for noncontact detection, while the best performance for AS is obtained with an air gap of 0.5 mm.

VI. Conclusion

In this article, we have successfully integrated MS and AS for contact and noncontact characterization of solid materials with a permittivity range of 1–6.15. The proposed sensor is based on a dual T-shaped resonator with a single port, which operates at $f_{r1} = 1.81$ GHz and $f_{r2} = 2.34$ GHz. In addition, the proposed device has independent characteristics, so that it can be used for contact and noncontact measurements separately. From the measurements, the average accuracy was 99.30% and 99.31% for MS and AS with an air gap (d) of 0.5 mm, respectively. The NS of the two sensors was 1.16% and 0.16%, while the range of the air gap (d) for AS was 0.5–1 mm. This integration of MS and AS can be recommended as an excellent solution for contact and noncontact material characterization in the biomedical, quality control, and materials science industries.

Acknowledgment

Syah Alam is with the Fakulti Kejuruteraan Elektronik dan Kejuruteraan Komputer (FKEKK), Universiti Teknikal Malaysia Melaka (UTeM), Durian Tunggal, Melaka 76100, Malaysia, and also with the Department of Electrical Engineering, Universitas Trisakti, West Jakarta 11440, Indonesia (e-mail: syah.alam@trisakti.ac.id).

Zahriladha Zakaria and Noor Azwan Shairi are with the Fakulti Kejuruteraan Elektronik dan Kejuruteraan Komputer (FKEKK), Universiti Teknikal Malaysia Melaka (UTeM), Durian Tunggal, Melaka 76100, Malaysia (e-mail: zahriladha@utem.edu.my).

Indra Surjati is with the Department of Electrical Engineering, Universitas Trisakti, West Jakarta 11440, Indonesia.

Mudrik Alaydrus is with the Department of Electrical Engineering, Universitas Mercubuana, West Jakarta 11650, Indonesia.

Teguh Firmansyah is with the Department of Electrical Engineering, Universitas Sultan Ageng Tirtayasa, Kota Serang, Banten 42124, Indonesia.

References

[1] M. H. Zarifi, H. Sadabadi, S. H. Hejazi, M. Daneshmand, and A. Sanati-Nezhad, "Noncontact and nonintrusive microwave-microfluidic flow sensor for energy and biomedical engineering," *Sci. Rep.*, vol. 8, no. 1, pp. 1–10, Jan. 2018, doi: 10.1038/s41598-017-18621-2.

[2] S. Kiani, P. Rezaei, M. Navaei, and M. S. Abrishamian, "Microwave sensor for detection of solid material permittivity in single/multilayer samples with high quality factor," *IEEE Sensors J.*, vol. 18, no. 24, pp. 9971–9977, Dec. 2018, doi: 10.1109/JSEN.2018.2873544.

[3] K. Solyom, P. R. Lopez, P. Esquivel, and A. Lucia, "Effect of temperature and moisture contents on dielectric properties at 2.45 GHz of fruit and vegetable processing by-products," *RSC Adv.*, vol. 10, no. 28, pp. 16783–16790, 2020, doi: 10.1039/c9ra10639a.

[4] C. Zhao, G. Wu, and Y. Li, "Measurement of water content of oil-water two-phase flows using dual-frequency microwave method in combination with deep neural network," *Measurement*, vol. 131, pp. 92–99, Jan. 2019, doi: 10.1016/j.measurement.2018.08.028.

[5] P. Jahangiri, M. Naser-Moghadasi, B. Ghalamkari, and M. Dousti, "A new planar microwave sensor for fat-measuring of meat based on SRR and periodic EBG structures," *Sens. Actuators A, Phys.*, vol. 346, Oct. 2022, Art. no. 113826, doi: 10.1016/j.sna.2022.113826.

[6] R. A. Alahnomi, Z. Zakaria, Z. M. Yussof, T. Sutikno, A. A. M. Bahar, and A. Alhegazi, "Determination of solid material permittivity using T-ring resonator for food industry," *Telkomnika*, vol. 17, no. 1, pp. 489–496, 2019, doi: 10.12928/TELKOMNIKA.v17i1.11636.

[7] S. Mohammadi and M. H. Zarifi, "Differential microwave resonator sensor for real-time monitoring of volatile organic compounds," *IEEE Sensors J.*, vol. 21, no. 5, pp. 6105–6114, Mar. 2021, doi: 10.1109/JSEN.2020.3041810.

[8] A. E. Omer et al., "Non-invasive real-time monitoring of glucose level using novel microwave biosensor based on triple-pole CSRR," *IEEE Trans. Biomed. Circuits Syst.*, vol. 14, no. 6, pp. 1407–1420, Dec. 2020, doi: 10.1109/TBCAS.2020.3038589.

[9] A. A. Abduljabar, N. Clark, J. Lees, and A. Porch, "Dual mode microwave microfluidic sensor for temperature variant liquid characterization," *IEEE Trans. Microw. Theory Techn.*, vol. 65, no. 7, pp. 2572–2582, Jul. 2017, doi: 10.1109/TMTT.2016.2647249.

[10] A. A. Abduljabar, H. Hamzah, and A. Porch, "Double microstrip microfluidic sensor for temperature correction of liquid characterization," *IEEE Microw. Wireless Compon. Lett.*, vol. 28, no. 8, pp. 735–737, Aug. 2018, doi: 10.1109/LMWC.2018.2849218.

[11] S. Kiani, P. Rezaei, and M. Navaei, "Dual-sensing and dual-frequency microwave SRR sensor for liquid samples permittivity detection," *Measurement*, vol. 160, Aug. 2020, Art. no. 107805, doi: 10.1016/j.measurement.2020.107805.

[12] F. Bagci, M. S. Gulsu, and B. Akaoglu, "Dual-band measurement of complex permittivity in a microwave waveguide with a flexible, thin and sensitive metamaterial-based sensor," *Sens. Actuators A, Phys.*, vol. 338, May 2022, Art. no. 113480, doi: 10.1016/j.sna.2022.113480.

[13] N. Rahman et al., "High quality factor using nested complementary split ring resonator for dielectric properties of solids sample," *Appl. Comput. Electromagn. Soc.*, vol. 35, no. 10, pp. 1222–1227, Dec. 2020, doi: 10.47037/2020.ACES.J.351016.

[14] C.-M. Chen, J. Xu, and Y. Yao, "Fabrication of miniaturized CSRR-loaded HMSIW humidity sensors with high sensitivity and ultra-low humidity hysteresis," *Sens. Actuators B, Chem.*, vol. 256, pp. 1100–1106, Mar. 2018, doi: 10.1016/j.snb.2017.10.057.

[15] K. Xu et al., "Novel microwave sensors based on split ring resonators for measuring permittivity," *IEEE Access*, vol. 6, pp. 26111–26120, 2018, doi: 10.1109/ACCESS.2018.2834726.

[16] S. P. Chakyar, S. K. Simon, C. Bindu, J. Andrews, and V. P. Joseph, "Complex permittivity measurement using metamaterial split ring resonators," *J. Appl. Phys.*, vol. 121, no. 5, Feb. 2017, Art. no. 054101, doi: 10.1063/1.4975111.

[17] A. Ebrahimi, J. Scott, and K. Ghorbani, "Transmission lines terminated with LC resonators for differential permittivity sensing," *IEEE Microw. Wireless Compon. Lett.*, vol. 28, no. 12, pp. 1149–1151, Dec. 2018, doi: 10.1109/LMWC.2018.2875996.

[18] G. Gugliandolo, K. Naishadham, G. Neri, V. C. Fernicola, and N. Donato, "A novel sensor-integrated aperture coupled microwave patch resonator for humidity detection," *IEEE Trans. Instrum. Meas.*, vol. 70, pp. 1–11, 2021, doi: 10.1109/TIM.2021.3062191.

[19] C. Wang et al., "High-accuracy complex permittivity characterization of solid materials using parallel interdigital capacitor—Based planar microwave sensor," *IEEE Sensors J.*, vol. 21, no. 5, pp. 6083–6093, Mar. 2021, doi: 10.1109/JSEN.2020.3041014.

[20] S. Lim, C. Kim, and S. Hong, "Simultaneous measurement of thickness and permittivity by means of the resonant frequency fitting of a microstrip line ring resonator," *IEEE Microw. Wireless Compon. Lett.*, vol. 28, no. 6, pp. 539–541, Jun. 2018, doi: 10.1109/LMWC.2018.2833202.

[21] A. Soltan, R. A. Sadeghzadeh, and S. Mohammad-Ali-Nezhad, "Microwave sensor for liquid classification and permittivity estimation of dielectric materials," *Sens. Actuators A, Phys.*, vol. 336, Apr. 2022, Art. no. 113397, doi: 10.1016/j.sna.2022.113397.

[22] M. Ndoye, I. Kerroum, D. Deslandes, and F. Domingue, "Air-filled substrate integrated cavity resonator for humidity sensing," *Sens. Actuators B, Chem.*, vol. 252, pp. 951–955, Nov. 2017, doi: 10.1016/j.snb.2017.06.101.

[23] S. Alam, Z. Zakaria, I. Surjati, N. A. Shairi, M. Alaydrus, and T. Firmansyah, "Dual-band independent permittivity sensor using single-port with a pair of U-shaped structures for solid material detection," *IEEE Sensors J.*, vol. 22, no. 16, pp. 16111–16119, Aug. 2022, doi: 10.1109/JSEN.2022.3191345.

[24] J. Yeo and J.-I. Lee, "Slot-loaded microstrip patch sensor antenna for high-sensitivity permittivity characterization," *Electronics*, vol. 8, no. 5, p. 502, May 2019, doi: 10.3390/electronics8050502.

[25] M. Behdani, M. M. H. Kalateh, H. Saghlatoon, J. Melzer, and R. Mirzavand, "High-resolution dielectric constant measurement using a sensor antenna with an allocated link for data transmission," *IEEE Sensors J.*, vol. 20, no. 24, pp. 14827–14835, Dec. 2020, doi: 10.1109/JSEN.2020.3012055.

[26] C. Li, T. Djerafi, E. Villeneuve, and K. Wu, "Planar antenna sensor with thermal stability for detection of ice formation," *Sens. Actuators A, Phys.*, vol. 341, Jul. 2022, Art. no. 113576, doi: 10.1016/j.sna.2022.113576.

[27] X. Yao, L. Tong, and Y. Cui, "A planar inverted-F antenna-based chemical sensor for ion concentrations," *Sens. Actuators Rep.*, vol. 2, no. 1, Nov. 2020, Art. no. 100006, doi: 10.1016/j.snr.2020.100006.

[28] H. Huang, F. Farahanipad, and A. K. Singh, "A stacked dual-frequency microstrip patch antenna for simultaneous shear and pressure displacement sensing," *IEEE Sensors J.*, vol. 17, no. 24, pp. 8314–8323, Dec. 2017, doi: 10.1109/JSEN.2017.2765893.

[29] C.-L. Yang, C.-S. Lee, K.-W. Chen, and K.-Z. Chen, "Noncontact measurement of complex permittivity and thickness by using planar resonators," *IEEE Trans. Microw. Theory Techn.*, vol. 64, no. 1, pp. 247–257, Jan. 2016, doi: 10.1109/TMTT.2015.2503764.

[30] L. Ali et al., "Design and optimization of microwave sensor for the non-contact measurement of pure dielectric materials," *Electronics*, vol. 10, no. 24, p. 3057, Dec. 2021, doi: 10.3390/electronics10243057.

[31] W.-J. Wu and G. Wang, "A modified AMC-based antenna sensor for contactless measurement of complex permittivity," *Measurement*, vol. 206, Jan. 2023, Art. no. 112261, doi: 10.1016/j.measurement.2022.112261.

[32] Q. Shi, X.-W. Xuan, H.-K. Nie, Z.-Y. Wang, and W. Wang, "Antenna sensor based on AMC array for contactless detection of water and ethanol in oil," *IEEE Sensors J.*, vol. 21, no. 19, pp. 21503–21510, Oct. 2021, doi: 10.1109/JSEN.2021.3102294.

[33] A. Ebrahimi, J. Scott, and K. Ghorbani, "Ultrahigh-sensitivity microwave sensor for microfluidic complex permittivity measurement," *IEEE Trans. Microw. Theory Techn.*, vol. 67, no. 10, pp. 4269–4277, Oct. 2019, doi: 10.1109/TMTT.2019.2932737.

[34] I. Piekarz, J. Sorocki, K. Wincza, and S. Gruszczynski, "Microwave sensors for dielectric sample measurement based on coupled-line section," *IEEE Trans. Microw. Theory Techn.*, vol. 65, no. 5, pp. 1615–1631, May 2017, doi: 10.1109/TMTT.2016.2641438.

[35] M. A. H. Ansari, A. K. Jha, and M. J. Akhtar, "Design and application of the CSRR-based planar sensor for noninvasive measurement of complex permittivity," *IEEE Sensors J.*, vol. 15, no. 12, pp. 7181–7189, Dec. 2015, doi: 10.1109/JSEN.2015.2469683.

[36] T. Haq, C. Ruan, S. Ullah, and A. K. Fahad, "Dual notch microwave sensors based on complementary metamaterial resonators," *IEEE Access*, vol. 7, pp. 153489–153498, 2019, doi: 10.1109/ACCESS.2019.2948868.

Alam, Syah

Universitas Trisakti, Jakarta, Indonesia 57191903622 https://orcid.org/0000-0002-0162-8364

174	48	8	View all metrics
Citations by ***128 documents***	Documents	*h*-index View *h*-graph	

Set alert Edit profile ••• More

Document & citation trends

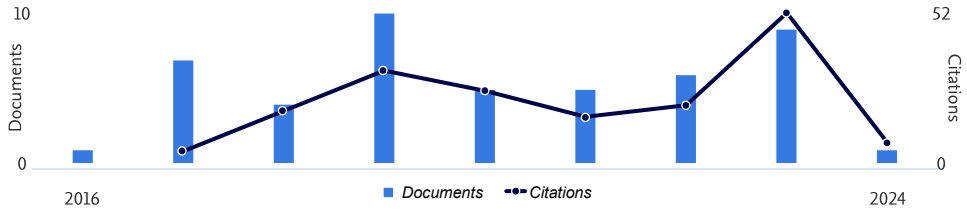

Scopus Preview

Scopus Preview users can only view a limited set of features. Check your institution's access to view all documents and features.

Check access

48 Documents	New Author Metrics	Cited by 128 documents	1 Preprint	65 Co-Authors	0 Topics	Beta 0 Awarded Grants

Note:

Scopus Preview users can only view an author's last 10 documents, while most other features are disabled. Do you have access through your institution? Check your institution's access to view all documents and features.

48 documents

Export all Save all to list Sort by Date (newest)

Article

Multifunctional Glass Microfluidic Microwave Sensor Attenuator for Detection of Permittivity and Conductivity With Device Protection

0 Citations

Firmansyah, T., Praptodiyono, S., Muttakin, I., ...Wibisono, G., Kondoh, J.

IEEE Sensors Journal, 2024, 24(4), pp. 4574–4585

Show abstract Related documents

Article

Modeling of quasi-tapered microstrip antenna based on expansion-exponential tapered method and its application for wideband MIMO structure

2 Citations

Firmansyah, T., Praptodiyono, S., Permana, J., ...Alaydrus, M., Kondoh, J.

AEU - International Journal of Electronics and Communications, 2023, 169, 154745

Show abstract Related documents

Article

Multifunctional of dual-band permittivity sensors with antenna using multicascode T-shaped resonators for simultaneous measurement of solid materials and data transfer capabilities

1 Citations

Alam, S., Zakaria, Z., Surjati, I., ...Alaydrus, M., Firmansyah, T.

Measurement: Journal of the International Measurement Confederation, 2023, 217, 113078

Show abstract Related documents

Article

Integrated Microwave Sensor and Antenna Sensor Based on Dual T-Shaped Resonator Structures for Contact and Noncontact Characterization of Solid Material

1 Citations

Alam, S., Zakaria, Z., Surjati, I., ...Alaydrus, M., Firmansyah, T.

IEEE Sensors Journal, 2023, 23(12), pp. 13010–13018

Show abstract Related documents

Review • *Open access*

A Compact and Low-Profile Curve-Feed Complementary Split-Ring Resonator Microwave Sensor for Solid Material Detection

6 Citations

Al-Gburi, A.J.A., Zakaria, Z., Abd Rahman, N., Alam, S., Said, M.A.M.

Micromachines, 2023, 14(2), 384

Show abstract Related documents

Conference Paper

Independent Permittivity Sensor Based on Dual T-Shaped Resonator for Solid Material Characterization

0 Citations

Alam, S., Shairi, N.A., Zakaria, Z., ...Surjati, I., Firmansyah, T.

2023 IEEE International Symposium on Antennas and Propagation, ISAP 2023, 2023

Show abstract Related documents

Article

Dual-Band MIMO Circular Patch Microstrip Antenna (CPMA) with Low Mutual Coupling for 5G Communication System

0 Citations

Putri, S.M., Surjati, I., Alam, S., ...Zakaria, Z., Firmansyah, T.

Journal of Nano- and Electronic Physics, 2023, 15(6), 06007

Show abstract Related documents

Article

COMPARISON PERFORMANCE ANALYSIS OF ATTENDANCE SYSTEM IN LOS AND NLOS CONDITIONS USING LORA, FSK, AND OOK MODULATION

0 Citations

Rahayu, Y., Hakiki, Y., Alam, S.

Journal of Engineering Science and Technology, 2023, 18, pp. 188–201

Show abstract Related documents

Article • *Open access*

WIDE BAND AND HIGH GAIN MICROSTRIP ANTENNA USING PLANAR SERIES ARRAY 4x2 ELEMENT FOR 5G COMMUNICATION SYSTEM

0 Citations

Alam, S., Surjati, I., Sari, L., ...Firmansyah, T., Zakaria, Z.

Eastern-European Journal of Enterprise Technologies, 2023, 4(5(124)), pp. 16–24

Show abstract Related documents

Conference Paper

Highly Independent Dual-Band Permittivity Sensors for Simultaneous Measurement of Solid Materials

0 Citations

Alam, S., Zakaria, Z., Surjati, I., ...Alaydrus, M., Firmansyah, T.

2023 33rd International Conference Radioelektronika, RADIOELEKTRONIKA 2023, 2023

Show abstract Related documents

Back to top

Author Position

Check your institution's access to view Author position.

Check access

First author %

Last author %

Co-author %

Corresponding author %

Single author %

View author position details

View list in search results format

View references

Set document alert

About Scopus

What is Scopus

Content coverage

Scopus blog

Scopus API

Privacy matters

Language

日本語版を表示する

查看简体中文版本

查看繁體中文版本

Просмотр версии на русском языке

Customer Service

Help

Tutorials

Contact us

ELSEVIER

IEEE Sensors Journal

COUNTRY

United States

Universities and research institutions in United States

Media Ranking in United States

SUBJECT AREA AND CATEGORY

Engineering
└ Electrical and Electronic Engineering

Physics and Astronomy
└ Instrumentation

PUBLISHER

Institute of Electrical and Electronics Engineers Inc.

H-INDEX

159

PUBLICATION TYPE

Journals

ISSN

1530437X

COVERAGE

2001-2023

INFORMATION

Homepage

How to publish in this journal

SCOPE

The fields of interest of the IEEE Sensors Journal are the theory, design , fabrication, manufacturing and applications of devices for sensing and transducing physical, chemical and biological phenomena, with emphasis on the electronics and physics aspect of sensors and integrated sensors-actuators. IEEE Sensors Journal deals with the following: -Sensor Phenomenology, Modelling, and Evaluation -Sensor Materials, Processing, and Fabrication -Chemical and Gas Sensors -Microfluidics and Biosensors -Optical Sensors -Physical Sensors: Temperature, Mechanical, Magnetic, and others -Acoustic and Ultrasonic Sensors -Sensor Packaging -Sensor Networks -Sensor Applications -Sensor Systems: Signals, Processing, and Interfaces -Actuators and Sensor Power Systems -Sensor Signal Processing for high precision and stability (amplification, filtering, linearization, modulation/demodulation) and under harsh conditions (EMC, radiation, humidity, temperature); energy consumption/harvesting -Sensor Data Processing (soft computing with sensor data, e.g., pattern recognition, machine learning, evolutionary computation; sensor data fusion, processing of wave e.g., electromagnetic and acoustic; and non-wave, e.g., chemical, gravity, particle, thermal, radiative and non-radiative sensor data, detection, estimation and classification based on sensor data) -Sensors in Industrial Practice

Quartiles

FIND SIMILAR JOURNALS

1	2	3	4
IEEE Sensors Letters	**Sensor Review**	**Chinese Journal of Sensors and Actuators**	**Sensors**
USA	GBR	CHN	CHE
87% similarity	**66%** similarity	**63%** similarity	**4** si

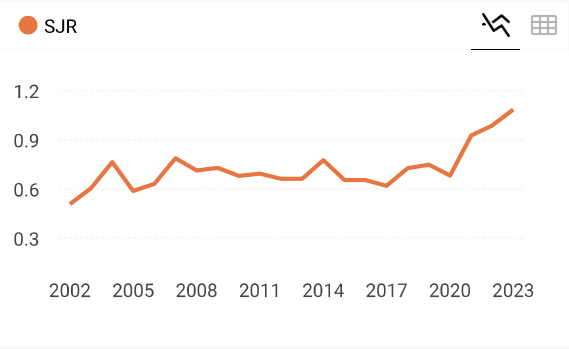

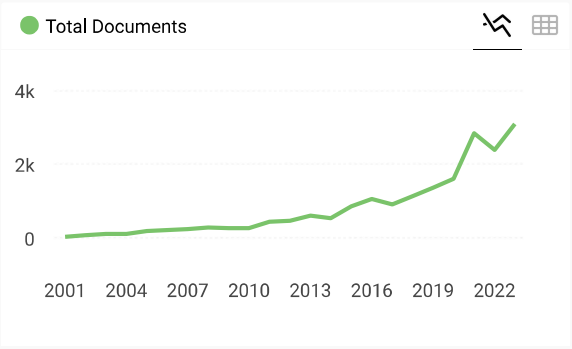

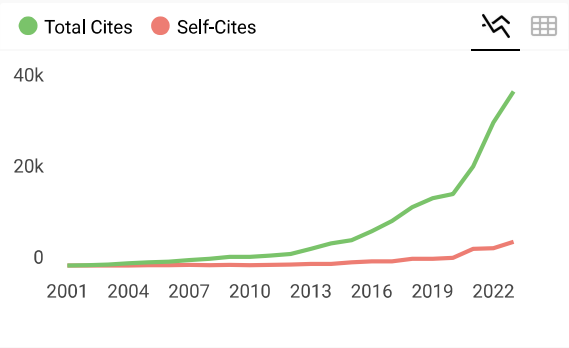

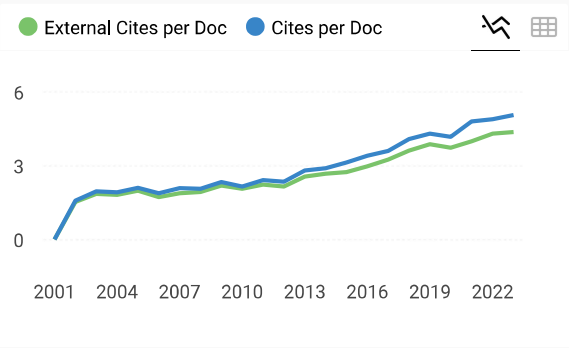

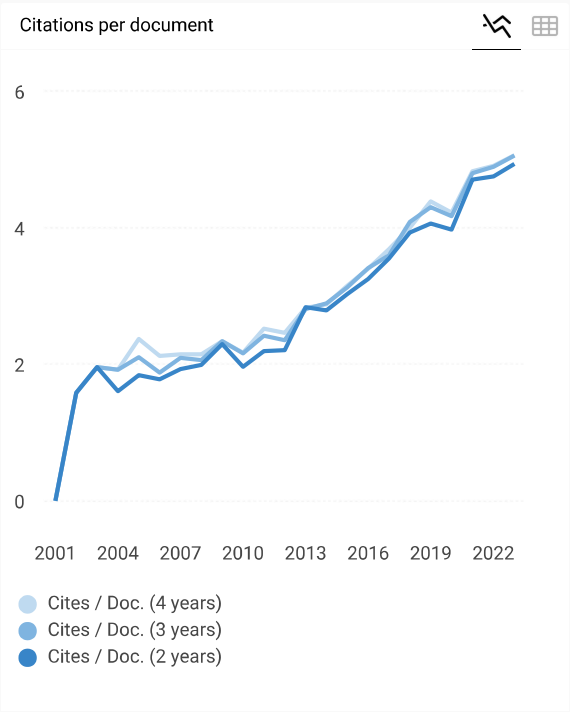

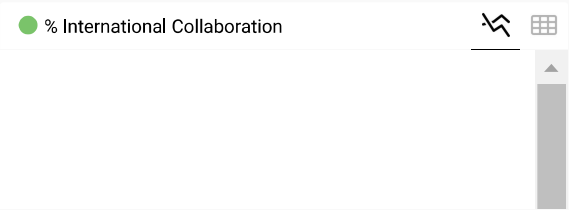

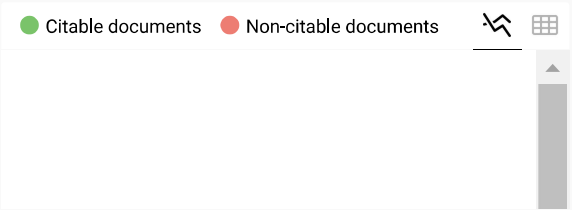

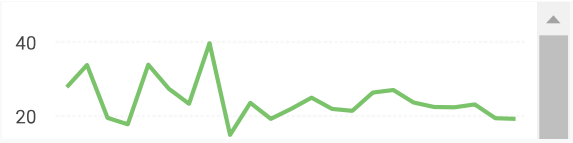

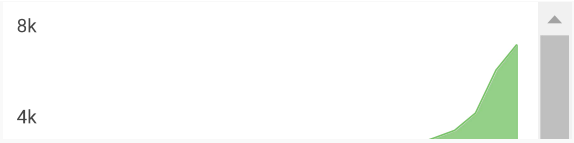

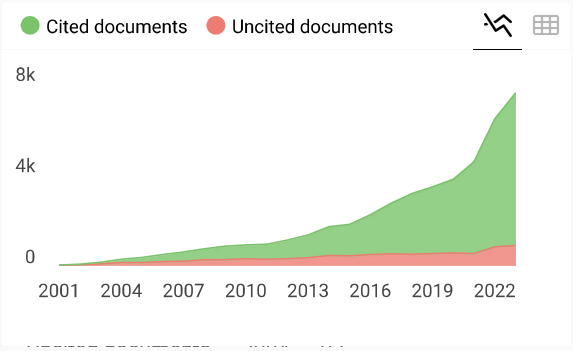

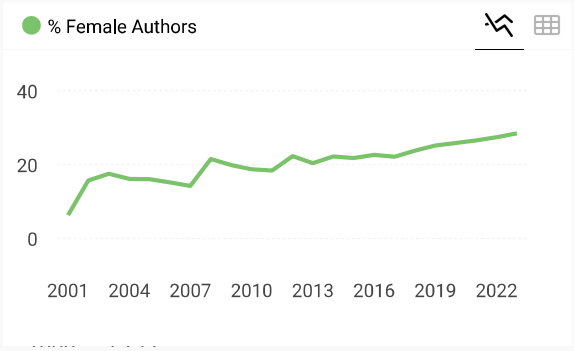

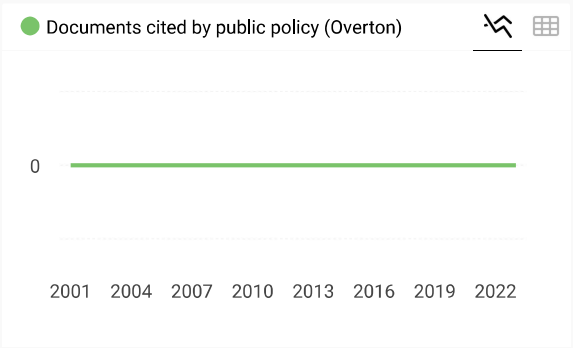

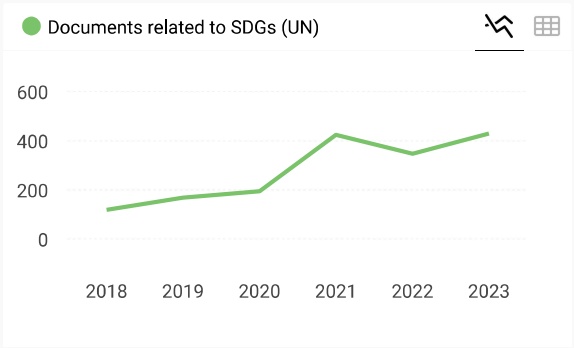

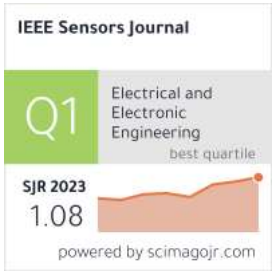

← Show this widget in your own website

Just copy the code below and paste within your html code:

<a href="https://www.scimag

SCImago Graphica

Explore, visually communicate and make sense of data with our **new data visualization tool**.

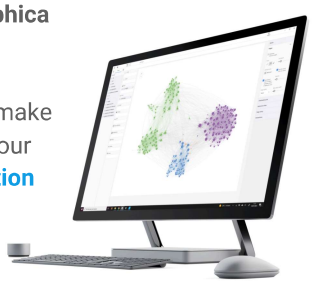

Metrics based on Scopus® data as of March 2024

Tayfun 2 years ago

Dear Colleagues,

Apart from this journal's website, how can I see the impact factor?
On the other hand, in the web of science, I see different quartile rankings (which is Q2, by the way) for IEEE Sensors Journal.

Could you please help me with this issue?

Best regards,

reply

Return to Search Results

EE SENSORS JOURNAL

Share This Journal

SN / eISSN **1530-437X / 1558-1748**
blisher **IEEE-INST ELECTRICAL ELECTRONICS ENGINEERS INC, 445 HOES LANE, PISCATAWAY, USA, NJ, 855-4141**

eneral Information

urnal Website	Visit Site
blisher Website	Visit Site
t Year Published	2001
equency	Semi-monthly
sues Per Year	24
untry / Region	UNITED STATES OF AMERICA
imary Language	English

eb of Science Coverage

Collection	Index	Category	Similar Journals
Core Collection	Science Citation Index Expanded (SCIE)	Engineering, Electrical & Electronic | Physics, Applied | Instruments & Instrumentation	Find Similar Journals
Current Contents	Engineering, Computing & Technology	Instrumentation & Measurement	Find Similar Journals
Other	Essential Science Indicators	Engineering	Find Similar Journals

arch a topic within this journal

Search a topic within this journal... Search

urnal Citation Report™ (JCR)

Journal Citation Reports™ 2023

Journal Impact Factor™ (JIF) JCR SUBSCRIPTION NOT ACTIVE

2022	2021
Not seeing a JIF? A JCR subscription is required to view the JIF for this journal. If this is an error, please use the “Check Subscription Status” button to contact support.	Not seeing a JIF? A JCR subscription is required to view the JIF for this journal. If this is an error, please use the “Check Subscription Status” button to contact support.
Categories: Engineering, Electrical & Electronic | Instruments & Instrumentation | Physics, Applied	**Categories:** Engineering, Electrical & Electronic | Instruments & Instrumentation | Physics, Applied

Check Subscription Status | Learn About Journal Citation Reports™

Journal Citation Indicator (JCI) NEW METRIC

The Journal Citation Indicator is a measure of the average Category Normalized Citation Impact (CNCI) of citable items (articles & reviews) published by a journal over a recent three year period. It is used to help you evaluate journals based on other metrics besides the Journal Impact Factor (JIF).

2022	2021
1.01	0.97
Categories: Engineering, Electrical & Electronic | Instruments & Instrumentation | Physics, Applied	**Categories:** Engineering, Electrical & Electronic | Instruments & Instrumentation | Physics, Applied

Learn About Journal Citation Indicator

eer Review Information

eb of Science Reviewer Recognition	Yes
aimed Reviews on Web of Science	47,879
blic Reports on Web of Science	No
gned Reports on Web of Science	No
ansparent Peer Review on ScholarOne	No

eate a free *Web of Science profile* to track your publications, citation metrics, peer reviews, and editing work for this journal.

ubMed® Information

dexed In	PubMed®
M® ID	101212357
rporate Author	Institute of Electrical and Electronics Engineers.|IEEE Sensors Council.

Criteria for selection of newly submitted titles and re-evaluation of existing titles in the Web of Science are determined by the Web of Science Editors in their sole discretion. If a publisher's editorial policy or business practices negatively impact the quality of a journal, or its role in the surrounding literature of the subject, the Web of Science Editors may decline to include the journal in any Clarivate product or service. The Web of Science Editors, in their sole discretion, may remove titles from coverage at any point if the titles fail to maintain our standard of quality, do not comply with ethical standards, or otherwise do not meet the criteria determined by the Web of Science Editors. If a journal is deselected or removed from coverage, the journal will cease to be indexed in the Web of Science from a date determined by the Web of Science Editors in their sole discretion – articles published after that date will not be indexed. The Web of Science Editors' decision on all matters relating to journal coverage will be final.

Clarivate.™ Accelerating innovation.